

Topological unidirectional guided resonances emerged from interband coupling

Xuefan Yin,¹ Takuya Inoue,¹ Chao Peng,^{2,3,*} and Susumu Noda^{1,†}

¹*Department of Electronic Science and Engineering, Kyoto University,
Kyoto-Daigaku-Katsura, Nishikyo-ku, Kyoto 615-8510, Japan*

²*State Key Laboratory of Advanced Optical Communication Systems and Networks, School of Electronics,
& Frontiers Science Center for Nano-optoelectronics, Peking University, Beijing, 100871, China*

³*Peng Cheng Laboratory, Shenzhen 518055, China*

(Dated: March 7, 2022)

Unidirectional guided resonances (UGRs) are optical modes in photonic crystal (PhC) slabs that radiate towards one side without the need for mirrors on the other, represented from a topological perspective by the merged points of paired, single-sided, half-integer topological charges. In this work, we report a mechanism to realize UGRs by tuning the interband coupling effect originating from up-down symmetry breaking. We theoretically demonstrate that a type of polarization singularity, the circular-polarized states (CPs), emerge from trivial polarization fields owing to the hybridization of two unperturbed states. By tuning structural parameters, two half-charges carried by CPs evolve in momentum space and merge to create UGRs. Our findings show that UGRs are ubiquitous in PhC slabs, and can systematically be found from our method, thus paving the way to new possibilities of light manipulation.

Unidirectional emission is of fundamental interest in research fields including non-Hermitian physics [1–3] and singular optics [4–6], and can benefit many realistic applications such as on-chip lasers [7–14] and energy-efficient grating couplers [15–20]. While most existing methods use mirrors made of metals or photonic-bandgap materials [21–23], or by utilizing the non-resonant blazing effect [24, 25] to forbid the radiation of light towards unnecessary ports, recent findings of unidirectional guided resonances (UGRs) [26, 27] revealed that an eigenstate itself can radiate towards only a single side of the photonic crystal (PhC) slab without the need for a mirror on the other. From the view of topological photonics [28–31], the UGRs were connected to polarization singularities [32–41] in momentum space, represented by topological charges [42–47]: they are the merged V points (vortex center of polarization fields) from paired C points (circular-polarized states) that carry the same signed half-integer topological charges on a single side. As reported, such half-charges can originate from splitting an integer charge carried by a bound state in the continuum (BIC) [42, 48–50] as $q = 1 \rightarrow 1/2 + 1/2$ [27, 51–53], or they can be spawned from “the void” as $q = 0 \rightarrow 1/2 + (-1/2)$ [47]. Both cases obey the conservation law of topological charges [42, 46, 50].

From such a topological view, the key to realizing UGRs is to create paired circular-polarized states (CPs). Although splitting from an integer charge of a BIC has been shown as a fairly intuitive example, it is still unclear how to deterministically separate and merge the CPs from the trivial polarization field, namely the void. Considering that the UGRs intrinsically do not depend on any symmetry, their realization is a formidable engineering challenge, especially when no appropriate BICs can be found as a starting point.

In this letter, we report a mechanism to realize UGRs without the premise of BICs. Specifically, we find that the interband couplings raised from up-down mirror symmetry breaking can be utilized as an effective degree of freedom (DOF) to hybridize the orthogonal bands in an unperturbed system.

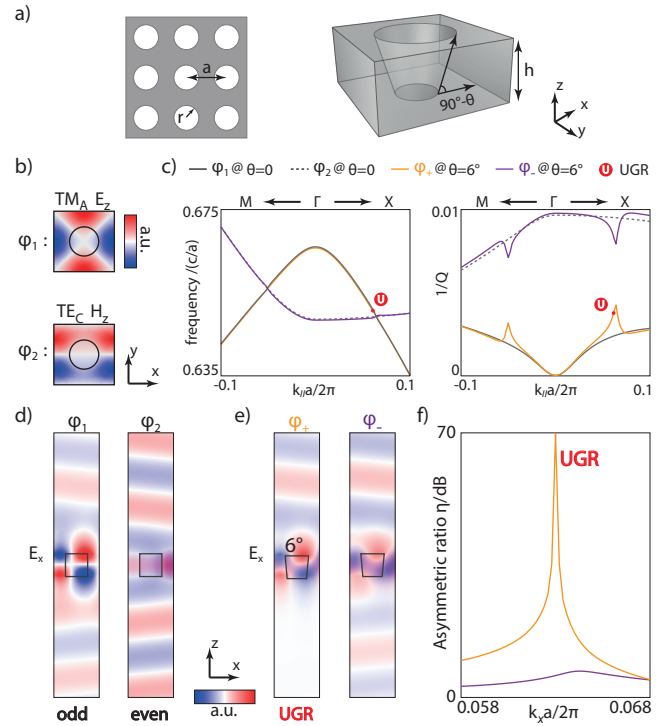


FIG. 1. UGR raised by interband coupling. a, schematic of a PhC slab, with slab thickness $h/a = 0.48$, radius $r/a = 0.238$. b, profiles of TM_A (φ_1) and TE_C (φ_2) modes. c, band structures of original resonances $\varphi_{1,2}$ (gray and gray dashed lines) and perturbed resonances $\varphi_{+,-}$ (yellow and purple lines) along the M- Γ -X direction, with a UGR at $(k_x = 0.063, k_y = 0)$ in φ_+ . d, e, profiles of $\varphi_{1,2}$ and $\varphi_{+,-}$ at $(k_x = 0.063, k_y = 0)$. f, asymmetric radiation ratio η of $\varphi_{+,-}$.

As a result of interband coupling, the paired CPs with opposite half-charge of $q = \pm 1/2$ are spawned from the void of $q = 0$ and evolve in momentum space by adjusting the interband coupling strength. In the case of a system also possessing in-plane mirror symmetry, a pair of mirror-positioned

half-charges with the same sign in single-sided radiation can merge at the high-symmetry lines in momentum space, thus generating UGRs.

To be more specific, we focus on a two-dimensional (2D) square-latticed PhC slab with symmetric upper and lower claddings. We break the up-down mirror symmetry of the PhC slab by isotropically tilting the sidewalls of the air holes. Consequently, interband coupling occurs between two crossing bands which are originally orthogonal to each other. When the interband coupling is strong enough, it could give rise to two perturbed eigenstates with nontrivial topology upon the radiation: a CP pair with oppositely-signed half-charges. By tuning the tilting angle, the half-charges continuously move and merge in the $\Gamma - X$ or $\Gamma - M$ directions, creating multiple UGRs. Our investigation shows that the UGRs are even more ubiquitous than expected, because band-crossing and corresponding interband coupling are quite common in PhC slabs regardless of their specific material and geometry, such as refractive-index contrast, slab thickness, and hole shape.

We start from a free-standing Si_3N_4 slab patterned with square-lattice air holes. The sidewalls of the air holes can be either perfectly vertical or isotropically tilted, measured by an angle θ (Fig. 1a). According to Bloch's theorem, the eigenstates are in the form of $U_{x,y,z} = E_{x,y,z}(\mathbf{r})e^{-ik_{\parallel}\mathbf{r}}e^{i\omega t}$ with in-plane wavevector $\mathbf{k}_{\parallel} = (k_x, k_y)\beta_0$ characterizing k_{\parallel} -momentum space, where $\beta_0 = 2\pi/a$ and a is the lattice constant. For vertical sidewalls, we focus on the TM_A mode (denoted as φ_1) and TE_C mode (denoted as φ_2) around the 2nd- Γ point (Fig. 1b). Note that in the band structures (Fig. 1c, gray lines and gray dashed lines), φ_1 and φ_2 cross at $(k_x = 0.064, k_y = 0)$ and $(k_x = 0.035, k_y = 0.035)$, respectively. Due to the up-down mirror symmetry, both φ_1 and φ_2 are eigenfunctions of parity operator $\hat{\mathbf{P}}_z$, but with opposite eigenvalues: φ_1 is odd with $\sigma_z = -1$; φ_2 is even with $\sigma_z = 1$ (Fig. 1c). Therefore, the orthogonality forbids any interband coupling between them during the band crossing.

Then, we slightly tilt the sidewalls, turning the cylindrical air holes into truncated cones with $\theta = 6^\circ$. Owing to up-down mirror symmetry breaking, φ_1 and φ_2 couple and give rise to two perturbed eigenstates φ_+ and φ_- [54]. As shown in Fig. 1c, the real parts of their frequencies cross while imaginary parts anti-cross. As confirmed in Fig. 1e, $\varphi_{+,-}$ no longer preserve definite z -parity, and thus the radiation becomes up-down asymmetric, characterized by an asymmetric radiation ratio $\eta = \gamma_t/\gamma_b$, where $\gamma_{t,b}$ are decay rates towards the top and bottom. A UGR is found at $(k_x = 0.063, k_y = 0)$ upon φ_+ band near one of the crossing points, with an asymmetric ratio of 70 dB (Fig. 1h).

To investigate the details of interband coupling, we derive a two-level model from perturbation theory. Specifically, we start from an up-down symmetric system, in which φ_1 and φ_2 are two eigenstates of the unperturbed Hamiltonian $\hat{\mathbf{H}}_0 = 1/\varepsilon_0(x, y)\nabla \times \nabla \times$ with eigenvalues $\lambda_{1,2}$ (other eigenstates are neglected). With the tilting, a perturbation $\Delta\hat{\mathbf{H}}$ is added as $\hat{\mathbf{H}} = \hat{\mathbf{H}}_0 + \Delta\hat{\mathbf{H}}$. The detailed formulation of $\hat{\mathbf{H}}$ and $\Delta\hat{\mathbf{H}}$ can be found in Supplementary Section 1.

Accordingly, the unperturbed eigenstates $\varphi_{1,2}$ can be utilized as a set of bases of subspace (φ_1, φ_2) to depict the perturbed Hamiltonian $\hat{\mathbf{H}}$ in a form of a 2×2 matrix:

$$\mathcal{H} = \begin{bmatrix} \langle \varphi_1 | \Delta\hat{\mathbf{H}} | \varphi_1 \rangle + \lambda_1 & \langle \varphi_1 | \Delta\hat{\mathbf{H}} | \varphi_2 \rangle \\ \langle \varphi_2 | \Delta\hat{\mathbf{H}} | \varphi_1 \rangle & \langle \varphi_2 | \Delta\hat{\mathbf{H}} | \varphi_2 \rangle + \lambda_2 \end{bmatrix} \quad (1)$$

and the hybrid eigenstates can be written as

$$\varphi_{+,-}(\mathbf{k}_{\parallel}) = a_{+,-}(\mathbf{k}_{\parallel})\varphi_1(\mathbf{k}_{\parallel}) + b_{+,-}(\mathbf{k}_{\parallel})\varphi_2(\mathbf{k}_{\parallel}) \quad (2)$$

with the superposition coefficients given by the eigenvectors $[a, b]_{+,-}^T$ of \mathcal{H} . According to Eq. S6, the perturbation $\Delta\hat{\mathbf{H}}$ is proportional to the odd function $\tan \theta \cdot z$, and thus the inner-product terms in matrix \mathcal{H} can be simplified as:

$$\langle \varphi_j | \Delta\hat{\mathbf{H}} | \varphi_k \rangle \propto \langle \varphi_j | z | \varphi_k \rangle \tan \theta = \kappa_{jk} \tan \theta \quad (3)$$

As a result, only the eigenstates with opposite z -parity can couple to each other through the anti-diagonal coupling terms. As illustrated in Fig. 1d, $\varphi_{1,2}$ fulfill this prerequisite.

Accordingly, the eigenvalues of \mathcal{H} can be derived as:

$$\lambda_{+,-} = \frac{\lambda_1 + \lambda_2}{2} \pm \sqrt{\frac{(\lambda_1 - \lambda_2)^2}{4} + \kappa_{12}\kappa_{21} \tan^2 \theta} \quad (4)$$

Obviously, there exists a critical angle θ_c with proper \mathbf{k}_{\parallel} for which $(\lambda_1 - \lambda_2)^2/4 + \kappa_{12}\kappa_{21} \tan^2 \theta_c = 0$, namely at which the complex eigenvalues $\lambda_{+,-}$ are degenerate. Such points are known as the exceptional points (EPs) [1, 55–60]: the complex crossing points of eigenvalues in parameter space $(\theta, \mathbf{k}_{\parallel})$. We obtain $\theta_c = 6.9^\circ$ along the Γ - X direction ($\mathbf{k}_{\parallel} = k_x$) for the PhC shown in Fig. 1. We further plot the complex band structures of $\varphi_{+,-}$ in parameter space (θ, k_x) , as presented in Fig. 2a. An isolated EP is found at $(\theta = 6.9^\circ, k_x = 0.064)$.

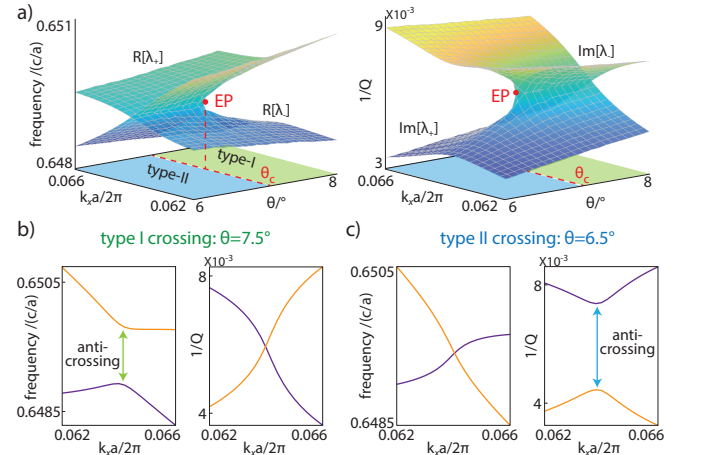


FIG. 2. Interband coupling scenario. a, band structures of perturbed resonances $\varphi_{+,-}$ in parameter space (θ, k_x) with k_y fixed to zero. Red dot denotes EP. b,c, examples of type-I and type-II crossings when $\theta = 7.5^\circ/6.5^\circ$.

As marked in Fig. 2a, the critical angle θ_c divides the parameter space (θ, k_x) into two different regions [61]:

Type-I crossing: for $\theta > \theta_c$, the real parts of $\lambda_{+,-}$ anti-cross and the imaginary parts cross (green region).

Type-II crossing: for $\theta < \theta_c$, the real parts of $\lambda_{+,-}$ cross and the imaginary parts anti-cross (blue region).

By continuously increasing θ from zero, the crossing type first belongs to type-II, and then transitions to type-I when passing by the EP at $\theta_c = 6.9^\circ$. In fact, similar transitions can be found not only along the Γ - X direction, but also along arbitrary k_{\parallel} directions in the Brillouin zone (BZ) due to C_4 symmetry. In Supplementary Section 2, we present the interband coupling scenario along $k_y = k_x/2$ direction as an example, for which the EP resides at ($\theta_c = 7.15^\circ, k_x = 0.0517$).

We further elaborate on the possibilities of creating polarization singularities from interband coupling. Eq. 2 shows that $\varphi_{+,-}$ are hybridized from $\varphi_{1,2}$. Accordingly, the far-field polarization of $\varphi_{+,-}$ also correlate to the polarization of $\varphi_{1,2}$ denoted by $d_{1,2}^s = c_{y;1,2}^s/c_{x;1,2}^s$. Here $c_{x,y;1,2}^s$ are the complex radiation amplitudes of $\varphi_{1,2}$ towards the top and bottom sides, marked by superscripts $s \in \{t, b\}$. From the two-level model, the polarization of $\varphi_{+,-}$ can be derived as:

$$d_{+,-}^s = m_{+,-}^s d_1^s + (1 - m_{+,-}^s) d_2^s, \quad s \in \{t, b\} \quad (5)$$

where $m_{+,-}^s$ are complex coefficients representing the interband coupling (a detailed discussion is provided in Supplementary Section 3). Obviously, the intrinsic radiation characteristics of perturbed eigenstates $\varphi_{+,-}$ are modified by the interband coupling effect. Once the polarization $d_{1,2}^s$ are linearly independent, polarization $d_{+,-}^s$ can be arbitrary values in principle if appropriate $m_{+,-}^s$ are applied.

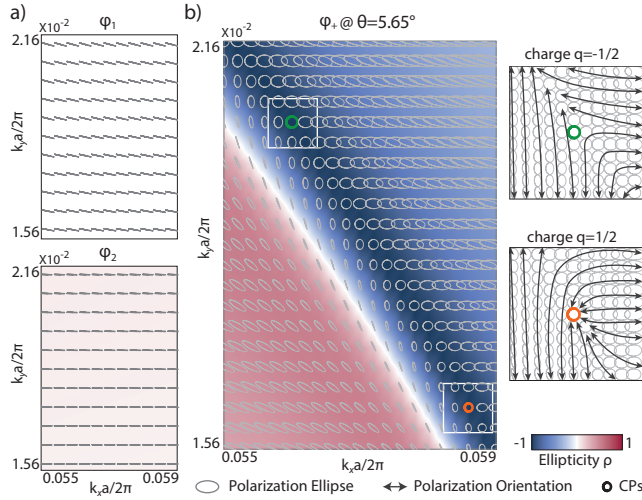


FIG. 3. CPs carrying half-charges emerged from interband coupling. a, downward polarization and ellipticity ρ of $\varphi_{1,2}$. b, left panel: downward polarization and ellipticity of perturbed resonance φ_+ when $\theta = 5.65^\circ$, where two CPs (green and orange circles) with ellipticity of -1 emerge. right panels: zoom-in windings of polarization orientation around the CPs.

Here we focus on a type of polarization singularity: CPs. Without loss of generality, we focus on the downward radiation of φ_+ . The condition of CP becomes $d_+^b = m_+^b(d_1^b - d_2^b) +$

$d_2^b = \pm i$. Clearly, two DOFs are necessary to fulfill this condition. In other words, the CPs can emerge in 2D parameter space, i.e. 2D k_{\parallel} -momentum space, by optimizing complex coefficient m_+^b (which also has 2 DOFs) from interband coupling even though $d_{1,2}^b$ themselves are trivial in polarization.

We plot the polarization ellipses and ellipticity ρ (colored map) [62] of $d_{1,2}^b$ in Fig. 3a, showing that both φ_1 and φ_2 are independent but near-linearly polarized with $\rho \approx 0$, namely no polarization singularities such as CPs are found. Then by tilting the sidewalls, complex coefficient m_+^b is induced from interband coupling, modifying the polarization of φ_+ . For a small θ , the coupling strength is not strong enough to create any CPs from trivial near-linear polarization, which we refer to as the void. When θ is increased to $\theta_v \sim 5.65^\circ$, a pair of CPs emerges simultaneously at ($k_x = 0.0554, k_y = 0.0212$) and ($k_x = 0.0588, k_y = 0.0159$) (Fig. 3b). It is noteworthy that the ellipticity of both CPs are identical as $\rho = -1$ (dark blue), showing that they are both left-handed CP (LCP).

The windings of polarization orientation [42] in the vicinity of two CPs are plotted in the right panel of Fig. 3b, showing that the two CPs carry half-charges with opposite polarity ($q = \pm 1/2$). Recalling the fact that when interband coupling is absent or sufficiently weak, φ_+ has no polarization singularity ($q = 0$), we conclude that the charge evolves as paired, opposite half-charges ($q = \pm 1/2$) carried by two LCPs spawned from the void ($q = 0$) as $0 \rightarrow 1/2 + (-1/2)$. Obviously, such an evolution obeys the conservation law of topological charges.

Next, we investigate how to merge two half-charges to create the UGRs. Before discussing the details, it is worthwhile to discuss the symmetry of system. As explained previously, under up-down mirror symmetry breaking, the polarization singularity of CPs, which appears for downward radiation of φ_+ , cannot coincide at the same k_{\parallel} point for upward radiation, and thus we can remain focused on $d_+(k_{\parallel})$. Owing to C_4 symmetry, a pair of opposite half-charges in one quadrant of momentum space would duplicate themselves to the other three quadrants, and evolve together under the constraint of C_4 symmetry. Notice that, to create UGRs, two half-charges with the same sign should be merged, which must come from different void points. Here, the in-plane mirror symmetries ensures paired mirror-positioned voids with respect to high-symmetry lines, providing the same signed half-charges pairs.

The detailed charge evolution of d_+^b is illustrated in Fig. 4a. Here we plot the right-half of momentum space. Owing to y -mirror symmetry, two pairs of CPs are spawned from two mirror-positioned voids when $\theta > \theta_v = 5.65^\circ$, and start to evolve from ($k_x = 0.057, k_y = \pm 0.0186$) (marked by stars), respectively. The CPs spawned from the same void have the same helicity but carry opposite half-charges. Recall that as a type of topological invariant, half-charges are robust in momentum space. By further increasing θ , the negative half-charges ($q = -1/2$) depart towards the far-end of the $\pm k_y$ directions, respectively (green lines), while the positive half-charges ($q = +1/2$) which originate from two different voids move towards each other (orange lines). At $\theta = 6^\circ$, the two positive half-charges meet on the k_x axis at

($k_x = 0.063, k_y = 0$), and merge into an integer topological charge as $1/2 + 1/2 \rightarrow +1$ (red U marker). Consequently, the downward radiation of φ_+ is completely forbidden and an upward radiating UGR emerges. For θ exceeding 6° , the integer charge $q = +1$ splits again into a pair of half-charges as $+1 \rightarrow 1/2 + 1/2$. Then, the half-charges depart away from each other and the UGR disappears.

The map of asymmetric ratio η for the UGR in d_+^b is plotted in Fig. 4b. The ratio reaches 70 dB at ($k_x = 0.063, k_y = 0$), which confirms the existence of UGR. As shown in the inset of Fig. 4b, a vortex is clearly observed in the polarization orientation fields of downward radiation, giving rise to an integer topological charge of $q = +1$ as expected.

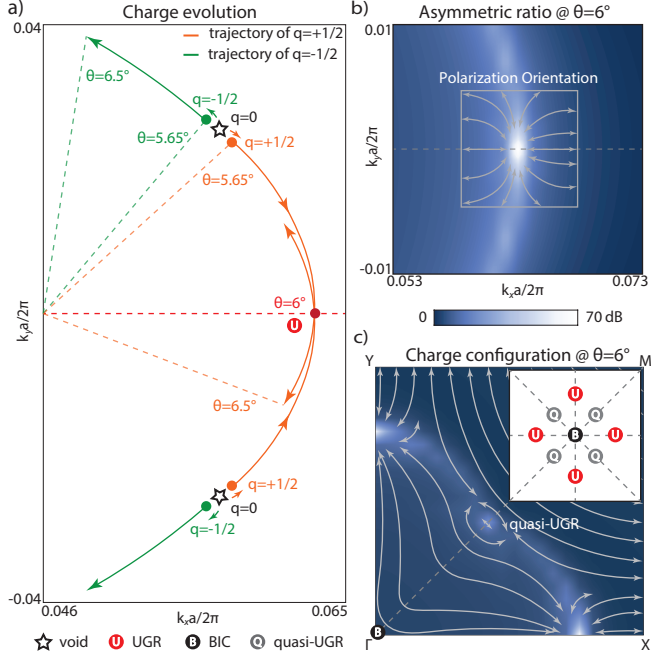


FIG. 4. UGRs emerged from interband coupling. a, Evolution of half-charges in d_+^b in right half of momentum space when θ is varied. b, Asymmetric radiation ratio (map) and the polarization orientation (arrows) around the UGR. c, Asymmetric radiation ratio (map) and the polarization orientation (arrows) in a quarter of momentum space. Inset: charge configuration in whole momentum space.

The role of in-plane mirror symmetry in creating UGRs is clearly shown in Fig. 4a: the trajectories of half-charges spawned from two mirror-positioned voids are symmetric with respect to the k_x axis, protected by y -mirror symmetry. Therefore, two positive half-charges steadily evolve toward each other and then merge at the k_x axis, creating UGRs along the $\Gamma - X$ direction. Similarly, x -mirror symmetry protects the trajectories with respect to the k_y axis, leading to the creation of UGRs along the $\Gamma - Y$ direction (Fig. 4c). Owing to C_4 symmetry, the $\Gamma - X$ and $\Gamma - Y$ directions are equivalent, and 4 UGRs emerge simultaneously in total as shown in the inset of Fig. 4c.

Besides the $\Gamma - X$ and $\Gamma - Y$ directions, $\Gamma - M$ directions are also high-symmetry lines owing to C_4 symmetry, and thus the

UGRs can be similarly found from merging two positive half-charges spawned from paired mirror-positioned voids with respect to the $\Gamma - M$ axes. However, recall the fact that the UGR in φ_+ is a result by hybridizing φ_1 and φ_2 . As shown in Fig. 1c, although the dispersion of φ_1 is fairly isotropic with respect to BZ center, the dispersion of φ_2 is considerably anisotropic. As a result, the condition of realizing UGRs in the $\Gamma - X$ and $\Gamma - M$ directions could be slightly different with respect to θ . In other words, when two positive half-charges merge in the $\Gamma - X$ direction, another pair of positive half-charges are close to but do not exactly arrive at the high-symmetry line in the $\Gamma - M$ direction (Fig. S3a). Consequently, the asymmetric radiation ratio is high but not infinite (Fig. S3b). We refer this kind of state as a “quasi-UGR”. A more detailed discussion can be found in Supplementary Section 4.

As shown in Fig. 4c, the UGRs emerge in the $\Gamma - X$ direction at $\theta = 6^\circ$ with $\eta = 70$ dB. For the same parameters, the highest asymmetric radiation ratio in the $\Gamma - M$ direction is $\eta = 25.8$ dB (Fig. S3b). As illustrated by the topological charge configuration (inset, Fig. 4c), there exist 1 BIC (Γ), 4 UGRs ($\Gamma - X, Y$), and 4 quasi-UGRs ($\Gamma - M$) in the BZ. Moreover, a high-asymmetric-radiation ring (colored map, Fig. 4c) emerges that connects those UGRs and quasi-UGRs.

It is noteworthy that C_4 symmetry is crucial for multiple UGRs, but it is not necessary for creating UGRs in general. In Supplementary Section 5, we reduce the in-plane symmetry from C_4 to y -mirror only, by changing the circular air holes to triangular ones (Fig. S5). As a result, a single isolated UGR is found at the k_x axis of ($k_x = 0.04, k_y = 0$) with $\eta = 68.3$ dB.

Until now, we have focused on the TM_A and TE_C modes as unperturbed bases (φ_1, φ_2) as shown in Fig. 1, and the band-crossing belongs to type-II when UGRs appear at $\theta = 6^\circ$. Given that any two modes with opposite z -parity are possible to couple, we turn to investigate another set of unperturbed bases, namely TM_C mode (denoted as φ_1) and TE_D mode (denoted as φ_2) near the 2nd- Γ point (left panel, Fig. 5a). It is readily confirmed that these modes fulfill the parity requirement of interband coupling.

Specifically, at a tilting angle of $\theta = 1.72^\circ$, type-I crossing can be identified from the complex band structures of Fig. 5a. An upward radiating UGR can be found upon the hybrid eigenstate φ_+ at ($k_x = 0.0172, k_y = 0$). The asymmetric radiation ratio η and charge configuration are presented in Fig. 5b. Clearly, 4 UGRs (red U markers) co-exist in the $\Gamma - X$ and $\Gamma - Y$ directions with η exceeding 70 dB, and together they form a high-asymmetric-radiation ring (upper panel of Fig. 5b). Further, we calculate the electric field profiles of two UGRs residing on the $+k_x$ and $+k_y$ axes (blue and green boxes in the lower panel of Fig. 5b) and plot them in Fig. 5c. Such UGRs are either y - or x -polarized, correspondingly.

Protected by in-plane mirror symmetry, the UGRs can robustly exist and continuously evolve along the high-symmetry lines [27] (detailed discussions are provided in Supplementary Section 6). For instance, by tuning the slab thickness h and hole radius r while fixing the tilting angle $\theta = 1.72^\circ$, the 4 off- Γ UGRs in Fig. 5b move towards the BZ center in an isotropic

manner. With $h/a \rightarrow 0.665$ and $r/a \rightarrow 0.217$, the UGRs merge at the Γ point, and the high-asymmetric-radiation ring shrinks into a point, as shown in Fig. 5d. As a result, the unidirectional radiation becomes vertical for both E_x and E_y components (Fig. 5d).

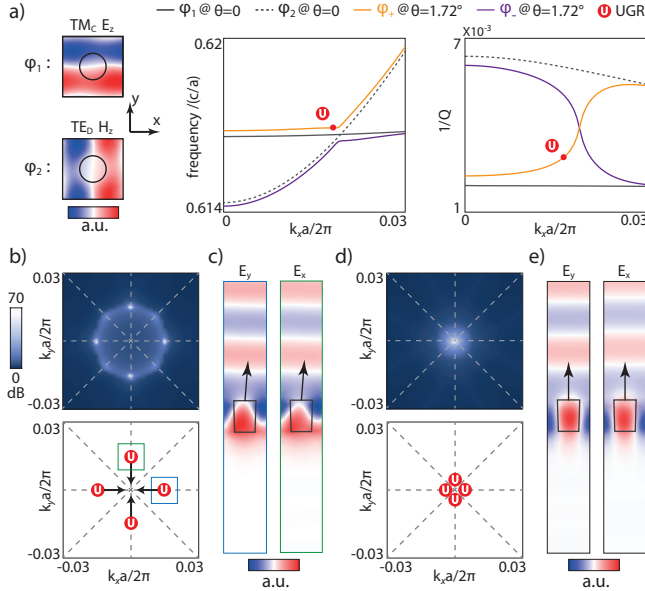


FIG. 5. Merging UGRs. a, left panels: profiles of TM_C (φ_1) and TE_C (φ_2) modes. right panels: band structures of original resonances $\varphi_{1,2}$ (gray and gray dashed lines) and perturbed resonances $\varphi_{+,-}$ (yellow and purple lines), with a UGR at ($k_x = 0.0172, k_y = 0$) in φ_+ when $h/a = 0.65$, $r/a = 0.219$ and $\theta = 1.72^\circ$. b, asymmetric radiation ratio and charge configuration of φ_+ . c, profiles of UGRs in φ_+ at ($k_x = 0.0172, k_y = 0$) (blue box) and ($k_x = 0, k_y = 0.0172$) (green box), respectively. d,e, asymmetric radiation ratio, charge configuration and profiles of merging UGRs in φ_+ at Γ point.

It is noteworthy that, although the UGRs raised from interband coupling involve two unperturbed eigenstates, their unidirectional emission behavior is an intrinsic characteristics of one perturbed eigenstate, which does not originate from the interference between two independently excited resonances [63, 64]. Furthermore, since the UGRs selectively close one of the radiation channels, they exhibit interesting and abnormal phenomena under external excitation [65], leading to various applications for light manipulation.

In conclusion, we have proposed a systematic method to realize UGRs in PhC slab by coupling two unperturbed eigenstates from up-down mirror symmetry breaking. We find that the CPs carrying paired, opposite-signed topological half-integer charges are spawned from the void through interband coupling and can be controlled to merge only at one side of PhC slab, thus creating a UGR. Our findings shed light upon new possibilities for creating and utilizing polarization singularities in momentum space, providing a vivid picture for manipulating the optical radiation [66] in various applications such as light trapping [67–69], generation of vortex beams [70–74] and polarization conversion [75].

The authors are grateful to Prof. B.S. Song, Dr. J. Gellata, Dr. Z. Zhang and Dr. Y. Hu for helpful discussions. This work was partially supported by Grant-in-Aid for JSPS Research Fellow (21F20356). C. Peng was supported from National Natural Science Foundation of China (61922004 and 62135001), National Key Research and Development Program of China (2020YFB1806405) and Major Key Project of PCL (PCL2021A04 and PCL2021A14). X. Yin was supported by Research Fellowships of the Japan Society for Promotion of Science.

* pengchao@pku.edu.cn

† snoda@qoe.kuee.kyoto-u.ac.jp

- [1] E. J. Bergholtz, J. C. Budich, and F. K. Kunst, Exceptional topology of non-hermitian systems, *Rev. Mod. Phys.* **93**, 015005 (2021).
- [2] D. Leykam, K. Y. Bliokh, C. Huang, Y. D. Chong, and F. Nori, Edge modes, degeneracies, and topological numbers in non-hermitian systems, *Phys. Rev. Lett.* **118**, 040401 (2017).
- [3] H. Shen, B. Zhen, and L. Fu, Topological band theory for non-hermitian hamiltonians, *Phys. Rev. Lett.* **120**, 146402 (2018).
- [4] M. R. Dennis, K. O'Holleran, and M. J. Padgett, Singular optics: optical vortices and polarization singularities, *Prog. Opt.* **53**, 293 (2009).
- [5] M. Soskin, S. V. Boriskina, Y. Chong, M. R. Dennis, and A. Desyatnikov, Singular optics and topological photonics, *J. Opt.* **19**, 010401 (2016).
- [6] G. J. Gbur, *Singular Optics* (CRC Press, 2016).
- [7] W. Streifer, D. Scifres, and R. Burnham, Analysis of grating-coupled radiation in gaas: Gaalas lasers and waveguides-i, *IEEE J. of Quantum Electron.* **12**, 422 (1976).
- [8] M. Meier, A. Mekis, A. Dodabalapur, A. Timko, R. Slusher, J. Joannopoulos, and O. Nalamasu, Laser action from two-dimensional distributed feedback in photonic crystals, *Appl. Phys. Lett.* **74**, 7 (1999).
- [9] M. Imada, S. Noda, A. Chutinan, T. Tokuda, M. Murata, and G. Sasaki, Coherent two-dimensional lasing action in surface-emitting laser with triangular-lattice photonic crystal structure, *Appl. Phys. Lett.* **75**, 316 (1999).
- [10] H. Matsubara, S. Yoshimoto, H. Saito, Y. Jianglin, Y. Tanaka, and S. Noda, Gan photonic-crystal surface-emitting laser at blue-violet wavelengths, *Science* **319**, 445 (2008).
- [11] K. Hirose, Y. Liang, Y. Kurosaka, A. Watanabe, T. Sugiyama, and S. Noda, Watt-class high-power, high-beam-quality photonic-crystal lasers, *Nat. Photon.* **8**, 406 (2014).
- [12] M. Yoshida, M. De Zoysa, K. Ishizaki, Y. Tanaka, M. Kawasaki, R. Hatsuda, B. Song, J. Gellata, and S. Noda, Double-lattice photonic-crystal resonators enabling high-brightness semiconductor lasers with symmetric narrow-divergence beams, *Nat. Mater.* **18**, 121 (2019).
- [13] R. Sakata, K. Ishizaki, M. De Zoysa, S. Fukuhara, T. Inoue, Y. Tanaka, K. Iwata, R. Hatsuda, M. Yoshida, J. Gellata, *et al.*, Dually modulated photonic crystals enabling high-power high-beam-quality two-dimensional beam scanning lasers, *Nat. Commun.* **11**, 3487 (2020).
- [14] R. Morita, T. Inoue, M. De Zoysa, K. Ishizaki, and S. Noda, Photonic-crystal lasers with two-dimensionally arranged gain and loss sections for high-peak-power short-pulse operation, *Nature Photon.* **15**, 311 (2021).

- [15] B. Wang, J. Jiang, and G. P. Nordin, Compact slanted grating couplers, *Opt. Express* **12**, 3313 (2004).
- [16] G. Roelkens, D. V. Thourhout, and R. Baets, High efficiency grating coupler between silicon-on-insulator waveguides and perfectly vertical optical fibers, *Opt. Lett.* **32**, 1495 (2007).
- [17] A. Mekis, S. Gloeckner, G. Masini, A. Narasimha, T. Pinguet, S. Sahni, and P. De Dobbelaere, A grating-coupler-enabled cmos photonics platform, *IEEE J. Sel. Top. Quant. Electron.* **17**, 597 (2011).
- [18] M. T. Wade, F. Pavanello, R. Kumar, C. M. Gentry, A. Atabaki, R. Ram, V. Stojanović, and M. A. Popović, 75% efficient wide bandwidth grating couplers in a 45 nm microelectronics cmos process, in *2015 IEEE Optical Interconnects Conference (OI)* (2015) pp. 46–47.
- [19] C. Sun, M. T. Wade, Y. Lee, J. S. Orcutt, L. Alloatti, M. S. Georgas, A. S. Waterman, J. M. Shainline, R. R. Avizienis, S. Lin, *et al.*, Single-chip microprocessor that communicates directly using light, *Nature* **528**, 534 (2015).
- [20] A. Michaels and E. Yablonovitch, Inverse design of near unity efficiency perfectly vertical grating couplers, *Opt. Express* **26**, 4766 (2018).
- [21] R. L. Roncone, L. Li, K. A. Bates, J. J. Burke, L. Weisenbach, and B. J. J. Zelinski, Design and fabrication of a single leakage-channel grating coupler, *Appl. Opt.* **32**, 4522 (1993).
- [22] D. Taillaert, P. Bienstman, and R. Baets, Compact efficient broadband grating coupler for silicon-on-insulator waveguides, *Opt. Lett.* **29**, 2749 (2004).
- [23] L. Zhu, W. Yang, and C. Chang-Hasnain, Very high efficiency optical coupler for silicon nanophotonic waveguide and single mode optical fiber, *Opt. Express* **25**, 18462 (2017).
- [24] W. Streifer, R. Burnham, and D. Scifres, Analysis of grating-coupled radiation in gaas: Gaalas lasers and waveguides-ii: Blazing effects, *IEEE J. of Quantum Electron.* **12**, 494 (1976).
- [25] J. M. Miller, N. de Beaucouudrey, P. Chavel, J. Turunen, and E. Cambriil, Design and fabrication of binary slanted surface-relief gratings for a planar optical interconnection, *Appl. Opt.* **36**, 5717 (1997).
- [26] H. Zhou, B. Zhen, C. W. Hsu, O. D. Miller, S. G. Johnson, J. D. Joannopoulos, and M. Soljačić, Perfect single-sided radiation and absorption without mirrors, *Optica* **3**, 1079 (2016).
- [27] X. Yin, J. Jin, M. Soljačić, C. Peng, and B. Zhen, Observation of topologically enabled unidirectional guided resonances, *Nature* **580**, 467 (2020).
- [28] L. Lu, J. D. Joannopoulos, and M. Soljačić, Topological photonics, *Nature Photon.* **8**, 821 (2014).
- [29] A. B. Khanikaev and G. Shvets, Two-dimensional topological photonics, *Nature Photon.* **11**, 763 (2017).
- [30] T. Ozawa, H. M. Price, A. Amo, N. Goldman, M. Hafezi, L. Lu, M. C. Rechtsman, D. Schuster, J. Simon, O. Zilberberg, *et al.*, Topological photonics, *Rev. Mod. Phys.* **91**, 015006 (2019).
- [31] H. Wang, S. K. Gupta, B. Xie, and M. Lu, Topological photonic crystals: a review, *Front. Optoelectron.* **13**, 50 (2020).
- [32] J. F. Nye, Lines of circular polarization in electromagnetic wave fields, *Proc. R. Soc. Lond., A Math. phys. sci.* **389**, 279 (1983).
- [33] F. Flossmann, K. O'Holleran, M. R. Dennis, and M. J. Padgett, Polarization singularities in 2d and 3d speckle fields, *Phys. Rev. Lett.* **100**, 203902 (2008).
- [34] T. Bauer, P. Banzer, E. Karimi, S. Orlov, A. Rubano, L. Marrucci, E. Santamato, R. W. Boyd, and G. Leuchs, Observation of optical polarization möbius strips, *Science* **347**, 964 (2015).
- [35] T. Fösel, V. Peano, and F. Marquardt, L lines, c points and chern numbers: understanding band structure topology using polarization fields, *New J. Phys.* **19**, 115013 (2017).
- [36] K. Y. Bliokh, M. A. Alonso, and M. R. Dennis, Geometric phases in 2d and 3d polarized fields: geometrical, dynamical, and topological aspects, *Rep. Prog. Phys.* **82**, 122401 (2019).
- [37] W. Chen, Y. Chen, and W. Liu, Singularities and poincaré indices of electromagnetic multipoles, *Phys. Rev. Lett.* **122**, 153907 (2019).
- [38] Z. Che, Y. Zhang, W. Liu, M. Zhao, J. Wang, W. Zhang, F. Guan, X. Liu, W. Liu, L. Shi, *et al.*, Polarization singularities of photonic quasicrystals in momentum space, *Phys. Rev. Lett.* **127**, 043901 (2021).
- [39] J. Ni, C. Huang, L.-M. Zhou, M. Gu, Q. Song, Y. Kivshar, and C.-W. Qiu, Multidimensional phase singularities in nanophotonics, *Science* **374**, eabj0039 (2021).
- [40] Q. Wang, C.-H. Tu, Y.-N. Li, and H.-T. Wang, Polarization singularities: Progress, fundamental physics, and prospects, *APL Photonics* **6**, 040901 (2021).
- [41] W. Liu, W. Liu, L. Shi, and Y. Kivshar, Topological polarization singularities in metaphotonics, *Nanophotonics* **10**, 1469 (2021).
- [42] B. Zhen, C. W. Hsu, L. Lu, A. D. Stone, and M. Soljačić, Topological nature of optical bound states in the continuum, *Phys. Rev. Lett.* **113**, 257401 (2014).
- [43] E. N. Bulgakov and D. N. Maksimov, Bound states in the continuum and polarization singularities in periodic arrays of dielectric rods, *Physical Review A* **96**, 063833 (2017).
- [44] Y. Zhang, A. Chen, W. Liu, C. W. Hsu, B. Wang, F. Guan, X. Liu, L. Shi, L. Lu, and J. Zi, Observation of polarization vortices in momentum space, *Phys. Rev. Lett.* **120**, 186103 (2018).
- [45] H. M. Doeleman, F. Monticone, W. den Hollander, A. Alu, and A. F. Koenderink, Experimental observation of a polarization vortex at an optical bound state in the continuum, *Nat. Photon.* **12**, 397 (2018).
- [46] W. Chen, Q. Yang, Y. Chen, and W. Liu, Evolution and global charge conservation for polarization singularities emerging from non-hermitian degeneracies, *Proc. Natl. Acad. Sci. U.S.A.* **118**, e2019578118 (2021).
- [47] Y. Zeng, G. Hu, K. Liu, Z. Tang, and C.-W. Qiu, Dynamics of topological polarization singularity in momentum space, *Phys. Rev. Lett.* **127**, 176101 (2021).
- [48] J. von Neuman and E. Wigner, Über merkwürdige diskrete Eigenwerte. Über das Verhalten von Eigenwerten bei adiabatischen Prozessen, *Physikalische Zeitschrift* **30**, 467 (1929).
- [49] D. Marinica, A. Borisov, and S. Shabanov, Bound states in the continuum in photonics, *Phys. Rev. Lett.* **100**, 183902 (2008).
- [50] C. W. Hsu, B. Zhen, A. D. Stone, J. D. Joannopoulos, and M. Soljačić, Bound states in the continuum, *Nat. Rev. Mater.* **1**, 16048 (2016).
- [51] W. Liu, B. Wang, Y. Zhang, J. Wang, M. Zhao, F. Guan, X. Liu, L. Shi, and J. Zi, Circularly polarized states spawning from bound states in the continuum, *Phys. Rev. Lett.* **123**, 116104 (2019).
- [52] W. Ye, Y. Gao, and J. Liu, Singular points of polarizations in the momentum space of photonic crystal slabs, *Phys. Rev. Lett.* **124**, 153904 (2020).
- [53] T. Yoda and M. Notomi, Generation and annihilation of topologically protected bound states in the continuum and circularly polarized states by symmetry breaking, *Phys. Rev. Lett.* **125**, 053902 (2020).
- [54] Y. Tanaka, T. Asano, Y. Akahane, B.-S. Song, and S. Noda, Theoretical investigation of a two-dimensional photonic crystal slab with truncated cone air holes, *Appl. Phys. Lett.* **82**, 1661 (2003).
- [55] W. Heiss, The physics of exceptional points, *J. Phys. Math. Gen.* **45**, 444016 (2012).
- [56] C. Dembowski, H.-D. Gräf, H. Harney, A. Heine, W. Heiss, H. Rehfeld, and A. Richter, Experimental observation of the

- topological structure of exceptional points, *Phys. Rev. Lett.* **86**, 787 (2001).
- [57] B. Zhen, C. W. Hsu, Y. Igarashi, L. Lu, I. Kaminer, A. Pick, S.-L. Chua, J. D. Joannopoulos, and M. Soljačić, Spawning rings of exceptional points out of dirac cones, *Nature* **525**, 354 (2015).
- [58] J. Doppler, A. A. Mailybaev, J. Böhm, U. Kuhl, A. Girschik, F. Libisch, T. J. Milburn, P. Rabl, N. Moiseyev, and S. Rotter, Dynamically encircling an exceptional point for asymmetric mode switching, *Nature* **537**, 76 (2016).
- [59] H. Zhou, C. Peng, Y. Yoon, C. W. Hsu, K. A. Nelson, L. Fu, J. D. Joannopoulos, M. Soljačić, and B. Zhen, Observation of bulk fermi arc and polarization half charge from paired exceptional points, *Science* **359**, 1009 (2018).
- [60] M.-A. Miri and A. Alu, Exceptional points in optics and photonics, *Science* **363** (2019).
- [61] F. Keck, H. Korsch, and S. Mossmann, Unfolding a diabolic point: a generalized crossing scenario, *J. Phys. A: Math. Gen.* **36**, 2125 (2003).
- [62] W. H. McMaster, Polarization and the stokes parameters, *Am. J. Phys.* **22**, 351 (1954).
- [63] W. Suh, Z. Wang, and S. Fan, Temporal coupled-mode theory and the presence of non-orthogonal modes in lossless multi-mode cavities, *IEEE J. Quantum Electron.* **40**, 1511 (2004).
- [64] C. J. Chang-Hasnain and W. Yang, High-contrast gratings for integrated optoelectronics, *Adv. Opt. Photon.* **4**, 379 (2012).
- [65] Z. Zhang, X. Yin, Z. Chen, F. Wang, W. Hu, and C. Peng, Observation of intensity flattened phase shifting enabled by unidirectional guided resonance, *Nanophotonics* **10**, 4467 (2021).
- [66] X. Yin and C. Peng, Manipulating light radiation from a topological perspective, *Photon. Res.* **8**, B25 (2020).
- [67] J. Jin, X. Yin, L. Ni, M. Soljačić, B. Zhen, and C. Peng, Topologically enabled ultrahigh-q guided resonances robust to out-of-plane scattering, *Nature* **574**, 501 (2019).
- [68] M. Kang, S. Zhang, M. Xiao, and H. Xu, Merging bound states in the continuum at off-high symmetry points, *Phys. Rev. Lett.* **126**, 117402 (2021).
- [69] Z. Chen, X. Yin, J. Jin, Z. Zheng, Z. Zhang, F. Wang, L. He, B. Zhen, and C. Peng, Observation of miniaturized bound states in the continuum with ultra-high quality factors, *Sci. Bull.* (2021).
- [70] Y. Shen, X. Wang, Z. Xie, C. Min, X. Fu, Q. Liu, M. Gong, and X. Yuan, Optical vortices 30 years on: OAM manipulation from topological charge to multiple singularities, *Light Sci. Appl.* **8**, 90 (2019).
- [71] C. Huang, C. Zhang, S. Xiao, Y. Wang, Y. Fan, Y. Liu, N. Zhang, G. Qu, H. Ji, J. Han, *et al.*, Ultrafast control of vortex microlasers, *Science* **367**, 1018 (2020).
- [72] Z.-Q. Yang, Z.-K. Shao, H.-Z. Chen, X.-R. Mao, and R.-M. Ma, Spin-momentum-locked edge mode for topological vortex lasing, *Phys. Rev. Lett.* **125**, 013903 (2020).
- [73] B. Wang, W. Liu, M. Zhao, J. Wang, Y. Zhang, A. Chen, F. Guan, X. Liu, L. Shi, and J. Zi, Generating optical vortex beams by momentum-space polarization vortices centred at bound states in the continuum, *Nat. Photon.* **14**, 623 (2020).
- [74] Z. Zhang, X. Qiao, B. Midya, K. Liu, J. Sun, T. Wu, W. Liu, R. Agarwal, J. M. Jornet, S. Longhi, *et al.*, Tunable topological charge vortex microlaser, *Science* **368**, 760 (2020).
- [75] Y. Guo, M. Xiao, and S. Fan, Topologically protected complete polarization conversion, *Phys. Rev. Lett.* **119**, 167401 (2017).